Invited Paper

The fractal shape of speckled darkness

Mark R. Dennis,[a] Kevin O'Holleran[b] and Miles J. Padgett[b]

[a] H H Wills Physics Laboratory, University of Bristol, Tyndall Avenue, Bristol BS8 1TL, UK
[b] Department of Physics & Astronomy, University of Glasgow, Glasgow, G12 8QQ, UK

ABSTRACT

Propagating three-dimensional speckle fields are threaded by random networks of nodal lines (optical vortices). We review our recent numerical superpositions of simulations of random plane waves modelling speckle (O'Holleran et al. *Phys. Rev. Lett.* in press), in which the nodal lines and loops were found to have the fractal structure of brownian random walks. We discuss this result, and its comparison with the discrete vortices of the $\mathbb{Z}_3$ lattice model for cosmic strings. We argue that the scaling depends on the geometry of small vortex loops and avoided crossings. The analytic statistics of these events, along with related singularities are discussed, and the densities of vorticity-vanishing points and anisotropy C lines are found explicitly.

Keywords: Optical vortex, speckle, three-dimensional, random walk, fractal

1. INTRODUCTION

Our understanding of optical speckle, as a natural interference phenomenon, has concentrated historically on the properties of the bright speckle regions, and much is known of the statistical properties of bright speckle.[1–3] The high degree of spatial coherence in these random fields does not only lead to bright regions, however; in particular, there are places of complete destructive interference, about which much can also be said. Here, we describe some features of the structure of this random darkness in three dimensions, based on the results of numerical experiments reported in Ref. 4.

The most general form of complete destructive interference in scalar optical fields are optical vortices, also called phase singularities, nodes and wave dislocations.[5–8] In two-dimensional fields – usually the transverse plane of a forward-propagating optical beam – these vortices are points where the complex amplitude is zero, the phase is undefined, and the whole 2π interval of phases are present in the neighborhood of the point, increasing $(+)$ or decreasing $(-)$ in a right-handed sense around the point. This sign is called the *topological charge* of the vortex point, and its sense gives the rotation direction of energy flow (Poynting vector) around the vortex. Such a two-dimensional field is shown in Fig. 1, where the dark vortex points occur in low-intensity regions around the bright speckles, and the phase wraps by 2π around each vortex.

Vortices are extended in three dimensions (as the beam propagates) along lines, around which the phase gradient, and optical energy flux, rotate, giving rise to a direction along the line. This direction, or topological current, is related to the sign of topological charge when the line pierces a plane: if the line pierces outwards, the sign of the intersecting vortex point is positive, and negative if inwards. In general, vortex lines can be curved,[5] and twisted,[8,9] although they are stationary in monochromatic fields.[5,10,11]

As a random field propagates, its vortex lines permeate the whole field, tangling up in highly nontrivial ways that are not well-understood. Very simply, a vortex line 'hairpin' – that is, a vortex line with a point whose tangent lies in the transverse plane – appears as the nucleation or annihilation of oppositely signed vortex points in the evolving transverse plane.[12] A pair of such hairpins can form a closed vortex loop in three dimensions, and in holographically-controlled fields, it has been established theoretically[13,14] and verified experimentally[15,16] that vortex loops can be knotted or linked (and infinite vortex lines can in principle be braided[17]). Closed vortex loops have been observed in experimental three-dimensional speckle fields, although knots and links have not been[4] (although we see no reason why it should not be physically impossible, however unlikely). We will consider here the large-scale shape of vortex lines in random optical fields, studied by numerical experiment described in the following.

Further author information: MRD E-mail: mark.dennis@physics.org

Complex Light and Optical Forces II, edited by David L. Andrews, Enrique J. Galvez, Gerard Nienhuis,
Proc. of SPIE Vol. 6905, 69050C, (2008) · 0277-786X/08/$18 · doi: 10.1117/12.764771

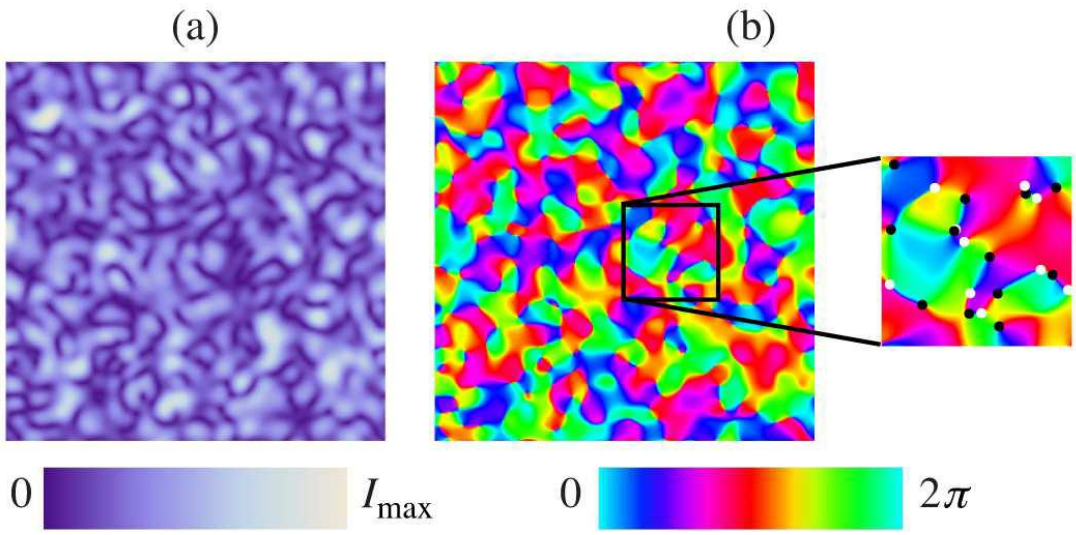

Figure 1. Figure demonstrating one transverse face of a Talbot cube: (a) intensity; (b) phase, with inset showing vortices, signed by strength, +1 (black), −1 (white). This is a superposition of random waves from a 27×27 k-space grid (spacing δk), with amplitudes modulated by a gaussian with variance K_σ given by Eq. (2).

As an additional parameter is changed, the vortex lines in a field move in a complicated way, and the vortex line topology may change by nucleation or annihilation of small loops, or reconnections (hyperbolic interchanges) of avoided crossings:[14,17–21] such an event has codimension 4, and does not naturally happen statically in three dimensions. Although one almost never finds a configuration with topology-changing event (such as reconnection), such events will occur after comparatively small perturbations, and therefore there will be a particular probability distribution for the avoided crossing range, or small loop area. This is the three-dimensional complex analog to the avoided crossing range of nodal lines studied in real chaotic wavefunctions in two-dimensional quantum billiards.[22] With loop nucleation and line reconnection, the global topology of the vortex configuration changes, for instance creating and dissolving vortex knots.[14,23]

Tangles of optical vortices in speckle are an example of a random quantized line process in physics; other such processes have been intensively studied, particularly tangles of quantized vortex lines in superfluids, which grow, coil and reconnect as the superfluid evolves nonlinearly.[24,25] Scaling aspects of the superfluid vortex configuration, both in real space[26–28] and Fourier space[27,29] reveal properties of the superfluid turbulence. Furthermore, there are analogies between superfluid vortex evolution and models of the evolution of cosmic strings in the early universe, which are also quantized defects.[30] Random optical fields, although displaying neither turbulence nor nonlinear dynamics, nevertheless have underlying structure which is revealed by the vortex configuration, and it is interesting to study the degree of similarity with these important systems from elsewhere in physics.

We discuss here the results of the numerical experiments described in Ref. 4. Random optical fields were simulated by linearly superposing many paraxial plane waves with random complex amplitudes, as is common in simulations of optical speckle[1,2,10] as well as other random physical fields such as condensed matter systems[31] and chaotic quantum eigenfunctions,[32] and the statistics of the local nodal geometry of such fields is well understood.[33] For each plane wave, with transverse wavevector $\boldsymbol{K}$, the random complex amplitudes was modulated by a gaussian power spectrum $\exp(-K^2/2K_\sigma^2)$, natural for speckle patterns, with K_σ the spectral standard deviation. However, unlike the usual random wave models where the directions of the superposed plane waves are also uniformly random, the plane waves in our superposition lie on a regular square lattice in the transverse k-plane, with spacing δk. The random fields resulting from this superposition are not only transversally periodic, but also periodic upon propagation by the Talbot effect (self-imaging effect)[34,35] – three-dimensional space is tiled by 'Talbot cubes' with side lengths $2\pi/\delta k$ in x and y, and $4\pi k_0/\delta k^2$ in z, where k_0 is the overall wavenumber and K_σ/k_0 the numerical aperture. The vortex line structure in the simulation is therefore finite and periodic,

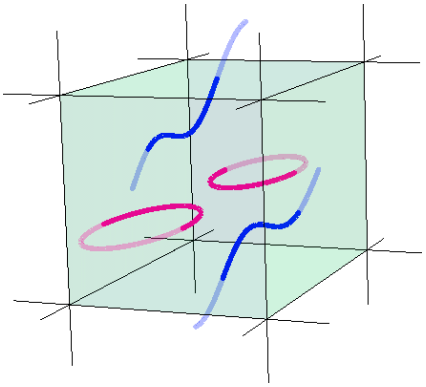

Figure 2. Schematic of three-dimensional Talbot cube, showing periodicity of vortex configuration. The purple line is a closed loop, the blue curve an infinite periodic line. The purple curve pierces the side of the Talbot cube at two points (corresponding to ± 1 strength vortices), and the blue curve pierces two sides, and top and bottom, before it repeats.

enabling the total topology to be completely determined: the vortices either form closed loops, or extend as infinite, periodic lines, and a single loop, or line period, may extend over many Talbot cubes. (These two possibilities can occur in superpositions of as few as four plane waves.[20]) From a numerical point of view this finiteness is very convenient, and this is an optical version of the periodic boundary conditions often imposed in physical simulations, where the dimensions of the cell are sufficiently large for bulk properties to dominate finiteness and edge effects. In our case, we looked for stabilization of the vortex point density in xy-, xz- and yz-planes, which is, for a continuous gaussian transverse spectrum,[8, 10, 36]

$$d_{xy} = \frac{K_\sigma^2}{2\pi}, \qquad d_{xz} = d_{yz} = \frac{K_\sigma^3}{2\pi k_0}. \tag{1}$$

The z-coordinate is then rescaled by defining natural lengthscales $\Lambda_x = \Lambda_y \equiv 2\pi/K_\sigma, \Lambda_z \equiv 2\pi k_0/K_\sigma^2$, and the vortex density in each plane becomes $2\pi/\Lambda^2$. Under this rescaling, the vortex tangle becomes isotropic, although the Talbot cube is still much longer in z than transversely. In our simulations, we superposed a 27×27 transverse k-space grid, with

$$K_\sigma = 0.003 k_0 = 3.9 \delta k. \tag{2}$$

Eq. (1) is an example of the analytic statistical calculations of local quantities possible in the continuum random wave model (as opposed to the discrete k-space model used for our numerics of large-scale properties). More complicated statistical expressions may be evaluated in a statistically simpler ensemble than random paraxially propagating waves, namely three-dimensional isotropic random waves.[11] Such isotropy is deeper than the mere rescaling described in the previous paragraph, which is equivalent to setting the second spectral moments equal in x, y and z; in an isotropic ensemble, all directions are completely equivalent. Such a field is not naturally optical (as there is no propagation direction but it is scalar) although it may be realized as a scalar component of an isotropic three-dimensional scalar field (such as a three-dimensional billiard[32]) or nonmonochromatic blackbody radiation,[37] in which vortex lines move.[11]

The structure of this article is as follows. In the next section, we discuss the fractality of vortex lines found in our simulated speckle patterns, especially in the context of brownian random walks (which have the same fractal dimension) and vortices in the $\mathbb{Z}_3$ model, a discrete complex scalar lattice model originally devised to describe the cosmic string configuration in the early universe[38] (which have the same dimension and loop length spectrum). In Section 3, we focus on the local geometry of small vortex loops and reconnection, which should determine aspects of the vortex line scaling. We also discuss the notions of vanishing-vorticity lines and anisotropy C lines, which are geometrically similar to C and L lines in nonparaxial polarization fields.[9, 39] Possible analytic statistical calculations in the isotropic random wave model follow in Section 4; although we are unable to derive expressions for small loops and reconnections, we provide calculations the density of anisotropy C lines and vanishing-vorticity lines (with technical details in Appendix A). We conclude in Section 5.

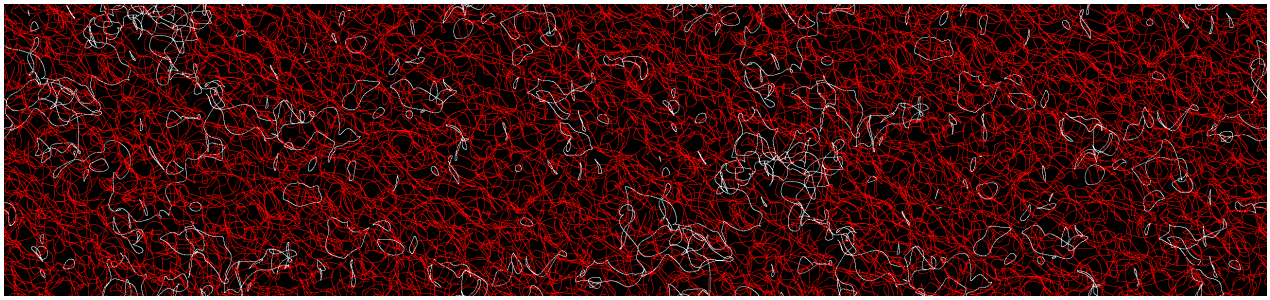

Figure 3. "Speckleghetti": numerically computed vortex configuration in a Talbot cube. The three-dimensional vortex structure has been projected into the yz-plane, the red curves representing infinite periodic lines, the white curves, closed vortex loops.

2. OPTICAL VORTEX LINES IN SPECKLE – A RANDOM WALK?

Fig. 3 is a realization of the tangled vortex structure occurring in a simulated Talbot cube. It is clear that most of the vortex line length is accounted for by infinite periodic lines, rather than closed loops. In fact, averaging over a large number of realizations, we found that about 72.7% of the total line length is accounted for by infinite periodic lines, and 27.3% of the lines are closed loops.

For a single such infinite vortex line, and an arbitrary point on it, we considered the dependence of the pythagorean distance R between points the line and the fixed point, as a function of the vortex arclength distance L between the same two points. This process is illustrated in Fig. 4, where, for an infinite periodic line, segments of the line (with the same starting point) for different orders of magnitude of L are plotted, along with a log-log plot of R against L for the same line. An illustration of the lines' traversal of three Talbot cubes is also shown. The arclength period of this line is comparatively short compared with most infinite periodic lines from our simulations.

Power-law scaling (i.e. a straight line in log-log plot) of R against L is the signature of a line's fractality[40]: in particular, the fractal dimension of the line is the reciprocal of the line's gradient. Notably, for a random walk on an n-dimensional lattice (for any $n > 1$), the exponent ν, where $R \propto L^{\nu}$ (i.e. ν is the gradient $\log R / \log L$), is $1/2$. That is, a random walk is a brownian fractal of dimension 2. Moreover, it has been shown[41] that random walks in one and two dimensions return to their origin with probability 1, and in three dimensions, the probability is

$$\text{Prob}_{\text{closed 3D random walk}} = 1 - \frac{32\pi^3}{\sqrt{6}\Gamma\left(\frac{1}{24}\right)\Gamma\left(\frac{5}{24}\right)\Gamma\left(\frac{7}{24}\right)\Gamma\left(\frac{11}{24}\right)} \approx 0.341. \tag{3}$$

If a random walk on a lattice is self-avoiding – that is, no lattice site is visited more than once – the scaling exponent ν is different. Roughly speaking, the random walk line is straighter as it cannot return to the same sites. For self avoiding random walks, the exponent ν is dimension-dependent: in 2D,[42] $\nu = 3/4$ and in 3D,[43] it is 0.588.

Fig. 5 shows the results of an extensive analysis of the R, L scalings of vortex lines in speckle. Firstly, for each line, plots such as Fig. 4(d) were averaged over different starting points on the line; this mean curve is rather smooth. Next, many such average curves, from different infinite lines, were superimposed: clearly, there is a range of approximately two orders of magnitude with fractal characteristics (the upper cutoff mainly occurs due to the infinite lines of shorter period – the range of fractality is higher for longer lines). In particular, we determine the fitted $\nu = 0.52 \pm 0.01$, extremely close to brownian fractality.

We find this a very striking result: nodal lines in three-dimensional linear random wave superpositions have the same degree of fractality as random walks, or three-dimensional brownian motion. In particular, this is somewhat surprising as vortex lines do not intersect themselves generically; as mentioned above, such a self-intersection would constitute a reconnection event, which almost never occurs. Therefore behavior closer to a self-avoiding random walk might be more expected. However, vortex lines may approach arbitrarily closely

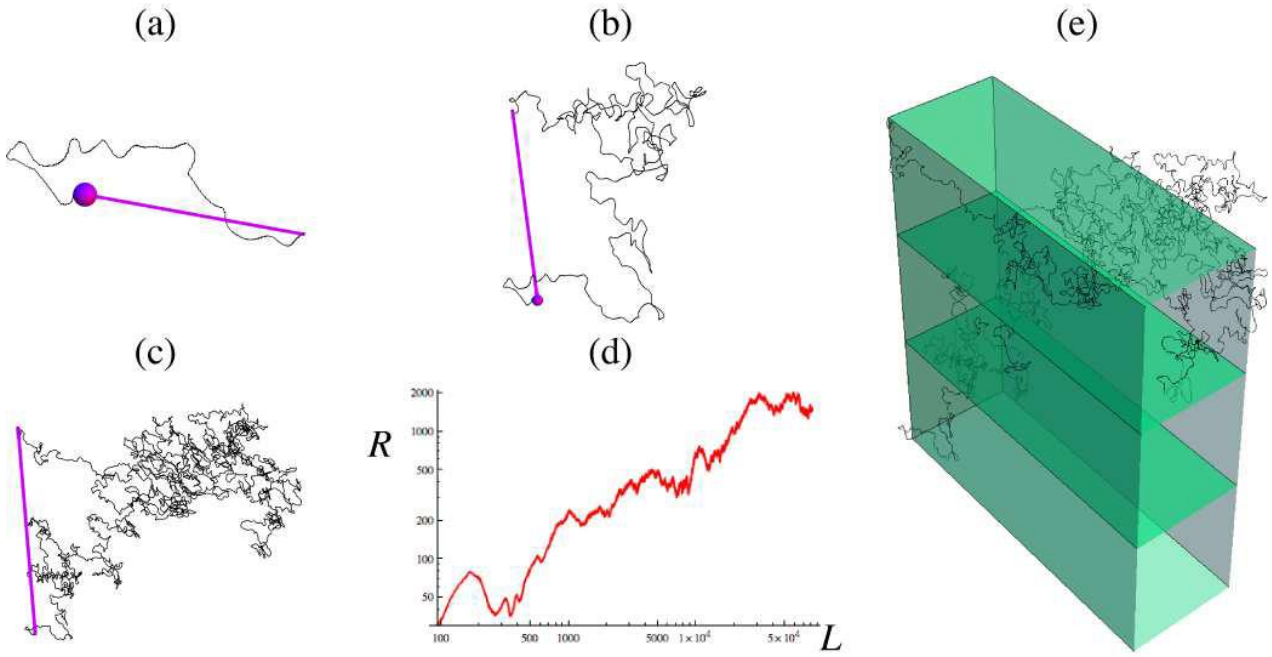

Figure 4. Figure showing the change in arclength L and pythagorean distance R from a fixed point on a random vortex line, at different scales in units of Λ: (a) $L = 860, R = 188$; (b) $L = 8260, R = 361$; (c) $L = 82605, R = 1494$ (the total length of the infinite periodic line). Part (d) shows a log-log plot of R against L for all values along this length. Part (e) is another representation of part (c) from a different direction, showing how the vortex line period relates to the tiling Talbot cubes. Of course, translations of this line occur in corresponding points in every Talbot cube.

without actually touching, resulting in 'avoided crossings' (as discussed in the next section); non-lattice random curves do not intersect themselves generically.[44]

In Ref. 4, we also compared the distribution of vortices in our speckle simulations with a natural lattice model of a three-dimensional complex field, the so-called $\mathbb{Z}_3$ model.[38] Each cube (square) face on a cubic (square) lattice is assigned uniformly randomly an integer $j = 0, 1$ or 2 (or, perhaps more evocatively, a phase factor $\exp(2\pi\,\mathrm{i}\,j)$). In two dimensions, such a process gives rise to discrete ± 1 topological charges at the vertices joining the lattice sites, when a loop around the neighboring squares or cubes encounters are a cyclic permutation of $(0, 0, 1, 2)$ (positive) or $(0, 0, 2, 1)$ (or an equivalent cycle of $\mathbb{Z}_3$). In three dimensions, this discrete topological charge becomes a topological current along lines, which is conserved, although pairs of lines can meet at unresolvable intersections. Examples of this random $\mathbb{Z}_3$ process in two- and three-dimensional lattices are illustrated in Fig. 6; we will refer to these quantized objects as $\mathbb{Z}_3$ vortices. The three-dimensional model was the basis in Ref. 38 as an ansatz for the distribution of U(1) cosmic strings in the early universe.*

In Ref. 38, the vortex intersections are broken at random (respecting the orientations of the two incoming, two outgoing $\mathbb{Z}_3$ vortex lines), giving rise to a network of well-defined lines, periodic if periodic boundary conditions are imposed on the supporting cubic lattice. The network of random $\mathbb{Z}_3$ vortices is then analyzed by the same fractal analysis described above for vortex lines[38] (on a $40 \times 40 \times 40$ periodic lattice), with resulting fractal dimension 2.00 ± 0.07, that is, brownian fractality again. Furthermore, numerous other power-law aspects of the $\mathbb{Z}_3$ vortex configuration are found in the paper, in particular the distribution of closed loops according to length (actually, perimeter of the bounding lattice cuboid), which is found to be -2.6 ± 0.1.[38] This result is justified by consistency with the theoretical scaling of $-5/2$ predicted by brownian fractality and scale invariance (the

*It is interesting to note that Halperin, in the acknowledgments section of his significant work[31] on the distribution of vortices in gaussian random fields, gives one of his motivations as understanding the creation of magnetic monopoles in the early universe.

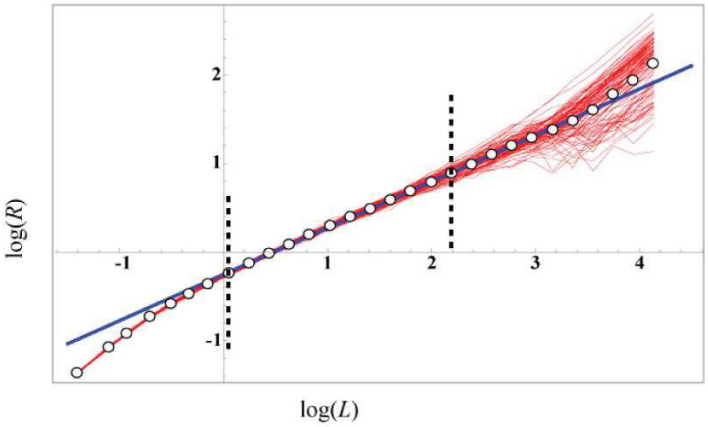

Figure 5. Figure showing plot of $\log R$ against $\log L$ for 100 infinite periodic optical vortex lines from different random superpositions. Each curve represents one periodic line, averaged over all possible starting points. The gradient of 0.52 ± 0.01, fitted over the marked range, strongly suggests a scale invariance over which the vortex lines have brownian characteristics. The upper limit of this range is solely a result of the periodicity of the Talbot cell. Figure based on Fig. 3 of Ref. 4.

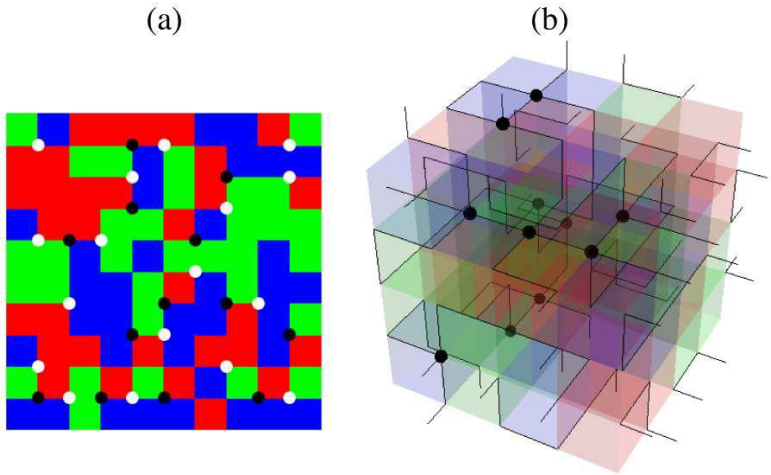

Figure 6. Illustrating the $\mathbb{Z}_3$ model (a) in two dimensions and (b) in three. The squares and cubes are assigned integers 0, 1, or 2 with uniform probability, represented by red, green, blue respectively. A vortex point (line) occurs if in a circuit of the four squares (cubes) around a vertex (edge) go through a monotonic cycle of $\mathbb{Z}_3$. This results in $\pm$ topological charges in two dimensions, and a network of oriented, intersecting lines in three (the intersections are represented by black spheres). Periodic boundary conditions are assumed on the $4 \times 4 \times 4$ cubic lattice in (b).

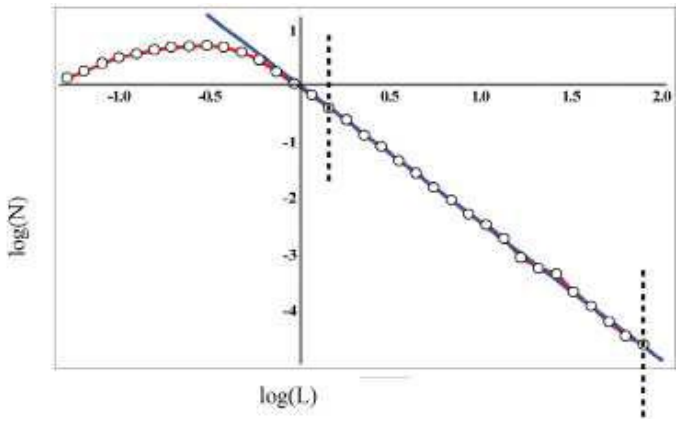

Figure 7. Log-log histogram of closed optical vortex loop length. The loops larger than a certain size have power-law (straight line) behavior, with exponent (gradient) fitted at -2.46 ± 0.02. Figure based on Fig. 4 of Ref. 4.

loop distribution does not change under a global rescaling of length). Motivated by this result, we computed from our simulations the number N of closed vortex loops according to their arclength L, with results given in Fig. 7: -2.46 ± 0.02, which is again close to $-5/2$. For $\mathbb{Z}_3$ vortices, the loop length scaling applied to loops of all lengthscales above the well-defined minimum size and below an upper cutoff.[38] On the other hand, from Fig. 7, it is evident that the smaller optical vortex loops do not follow this scaling; this is consistent with the fact that on the smaller lengthscales, vortex lines are reasonably smooth (i.e. far from brownian). The precise number of small loops is determined by the measure in probability space of configurations near the other topology-changing event, namely loop nucleation/annihilation. More details of this geometry are given in the next section.

If the distribution of vortices (optical or $\mathbb{Z}_3$) is truly scale-invariant, then the periodic lines are purely a finite-size effect, and so the fraction f of vortex line length (that is, infinite periodic lines) ought to scale with system size S as $S^{-1} \log S$. For $\mathbb{Z}_3$ strings, the fraction $f_{\mathbb{Z}_3}$, rather than decreasing with S, was found instead to approach ≈ 0.8 (considering a lattice of side length of up to 40).[38] Similarly, we found a similar stability of the infinite line fraction at $f_{\text{optical}} = 0.727 \pm 0.035$ (based on the vortex data from 88 fully-resolved Talbot cubes). Therefore, although neither vortex model appears to be truly scale-invariant (even within a suitable size range), both models have a similar value for f; the small numerical difference may be explained by the fact that the size of the $\mathbb{Z}_3$ lattice considered in Ref. 38 was equal in each direction, whereas our Talbot cubes are rather longer in the propagation direction than the transverse plane. It is also interesting to note that the fraction f can be compared with the probability that a three-dimensional random lattice walk does not close, which is 0.659 by Eq. (3).

There is a further tantalizing aspect of the connection between vortex scaling rules in three-dimensional optical speckle and the $\mathbb{Z}_3$ lattice model: a similar connection has been seen before in the scaling between nodal domains of chaotic monochromatic waves in two dimensions, and two-dimensional percolation on a lattice.[45] Despite objections,[46] the connection appears robust,[47] although a proof is still lacking. If the $\mathbb{Z}_3$ model statistics really provide a discretization of those of complex scalar wave fields, then the similarities between the results of Refs. 4, 38 may be the first steps in a generalization of random wave percolation to three dimensions and complex waves.

3. THE FIELD NEAR TOPOLOGY-CHANGING POINTS

The question of the global topology and fractal nature of nodal lines in random three-dimensional fields is closely related to the geometry of small nodal rings and reconnections. As described above, the actual topology-changing events (loop nucleation/annihilation and reconnection) are codimension 4, and occur generically only with the variation of an additional parameter.[14, 19, 23] However, perturbations of these events do occur in static three-dimensional fields, and small vortex rings and avoided crossings (hyperbolic close approaches) of vortex lines may

be analyzed in this way. The following discussion relates to Ref. 21, where the general geometry of topological events was considered in detail.

Let the complex scalar function representing the optical field be denoted $\psi(\mathbf{r}) = \xi(\mathbf{r}) + \mathrm{i}\,\eta(\mathbf{r})$; vortex lines occur along the locus $\psi = 0$. Furthermore, the three-dimensional field gradients are denoted as follows:

$$\boldsymbol{Z} \equiv \nabla\psi = \nabla\xi + \mathrm{i}\,\nabla\eta \equiv \boldsymbol{X} + \mathrm{i}\,\boldsymbol{Y}. \tag{4}$$

It is well-known[8, 11] that the vortex line tangent is given by the vorticity $\boldsymbol{\Omega}$:

$$\boldsymbol{\Omega} \equiv \frac{1}{2}\,\mathrm{Im}\,\boldsymbol{Z}^* \times \boldsymbol{Z} = \boldsymbol{X} \times \boldsymbol{Y}. \tag{5}$$

The vorticity $\boldsymbol{\Omega}$ is a vector field defined at every point in the space, not only on vortex lines.

Vortex topology-changing points occur when, on vortex lines, the tangent direction is undefined ($\boldsymbol{\Omega} = 0$). The locus $\boldsymbol{\Omega} = 0$ also occurs along lines, *vorticity-vanishing* lines (referred to as $\boldsymbol{\Omega} = 0$ lines in Ref. 21, and anisotropy L lines in Ref. 9, due to their morphological similarity with L lines in three-dimensional polarization fields,[39, 48] as discussed below).

The points on vorticity-vanishing lines on which the vortex topology changes satisfy the condition $\nabla|\psi|^2 = 0$; that is, stationary points of intensity.[21] Of course, the intensity is also stationary (at zero) along vortex lines, but vortex lines and vorticity-vanishing lines only cross at topology changing points. The Taylor expansion of ψ around such an intensity critical point (translated to the origin) is

$$\psi(\boldsymbol{r}) = \psi_0 + \boldsymbol{Z}_0 \cdot \boldsymbol{r} + \frac{1}{2}\boldsymbol{r} \cdot \boldsymbol{\Psi} \cdot \boldsymbol{r} + ..., \tag{6}$$

where the complex vector $\boldsymbol{Z}_0^* \times \boldsymbol{Z}_0 = 0$, and $\boldsymbol{\Psi} = \boldsymbol{\Xi} + \mathrm{i}\,\boldsymbol{\Upsilon}$ is the complex symmetric matrix of second derivatives. Choosing a coordinate system such that $\boldsymbol{Z}_0 = a\hat{\boldsymbol{z}}$ for c some complex number (this can be done since $\boldsymbol{Z}_0^* \times \boldsymbol{Z}_0 = 0$), the condition $\nabla|\psi|^2 = 0$ implies that $\mathrm{Re}\,c^*\psi_0 = 0$.[†] It is therefore possible to locally gauge-transform ψ by a phase factor $\psi \to \psi'$, where

$$\psi'(\boldsymbol{r}) = t + \mathrm{i}\,az + \frac{1}{2}\boldsymbol{r} \cdot \boldsymbol{\Psi} \cdot \boldsymbol{r} + ..., \tag{7}$$

where t and a are real ($\boldsymbol{\Psi}$ has not been relabelled). At a topology-changing point, $t = 0$ (its nature – ring or reconnection – is determined by $\boldsymbol{\Psi}$), and small rings and avoided crossings therefore occur when t is small.

When t is small, there are vortices near the intensity critical point, which are found from the intersection of the real and imaginary parts of Eq. (7), set to zero:

$$\begin{aligned} 0 &= t + \frac{1}{2}\boldsymbol{R} \cdot \boldsymbol{\Xi}_\perp \cdot \boldsymbol{R} + z\boldsymbol{P} \cdot \boldsymbol{R} + \frac{1}{2}z^2\Xi_{zz}, \\ 0 &= az + \frac{1}{2}\boldsymbol{R} \cdot \boldsymbol{\Upsilon}_\perp \cdot \boldsymbol{R} + z\boldsymbol{Q} \cdot \boldsymbol{R} + \frac{1}{2}z^2\Upsilon_{zz}, \end{aligned} \tag{8}$$

with

$$\boldsymbol{r} = \{\boldsymbol{R}, z\}, \quad \boldsymbol{R} = \{x, y\}, \quad \boldsymbol{\Xi}_\perp + \mathrm{i}\,\boldsymbol{\Upsilon}_\perp = \boldsymbol{\Psi}_\perp = \begin{pmatrix} \Psi_{xx} & \Psi_{xy} \\ \Psi_{xy} & \Psi_{yy} \end{pmatrix}, \quad \boldsymbol{P} = \{\Xi_{xz}, \Xi_{yz}\}, \quad \boldsymbol{Q} = \{\Upsilon_{xz}, \Upsilon_{yz}\}. \tag{9}$$

As described in Ref. 21, these equations completely determine the geometry of the avoided crossing or small loop.

The second equation of Eqs. (8), on rearranging slightly, gives

$$z = -\frac{\boldsymbol{R} \cdot \boldsymbol{\Upsilon}_\perp \cdot \boldsymbol{R}}{a + \boldsymbol{Q} \cdot \boldsymbol{R}} + \text{higher terms}. \tag{10}$$

[†]The casual reader is warned that in this section, local coordinates are chosen based on the local singularity geometry, as in Ref. 21, and not based on propagation direction, as in the previous section.

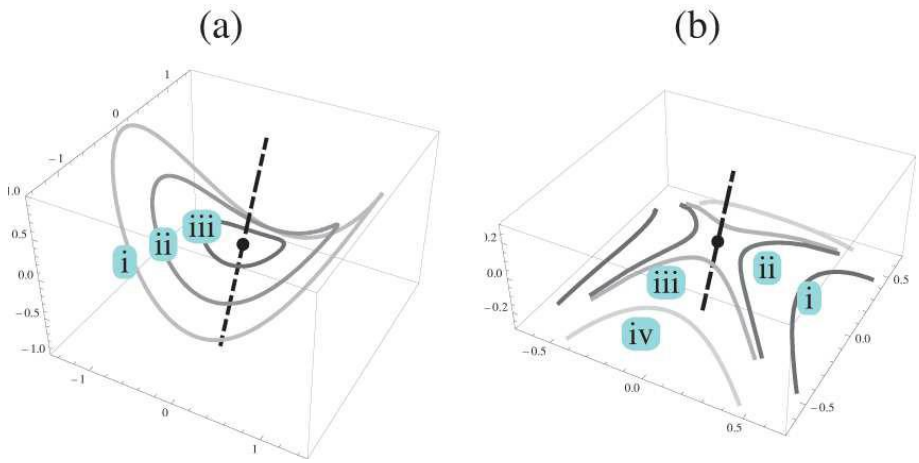

Figure 8. Examples of the two vortex topology-changing events. (a) Vortex loop nucleation/annihilation; parameters $\Psi_{11} = 1 - \mathrm{i}, \Psi_{22} = 2 + \mathrm{i}, \Psi_{12} = \Psi_{13} = 0, \Psi_{23} = -1, \Psi_{33}$ arbitrary, and i: $t = -1$; ii: $t = -0.5$; iii: $t = -0.1$. (b) Avoided crossings/reconnection; parameters $\Psi_{11} = 1 + \mathrm{i}, \Psi_{22} = -1 + \mathrm{i}, \Psi_{12} = \Psi_{13} = 0, \Psi_{23} = 0.5, \Psi_{33}$ arbitrary, and i: $t = -0.1$; ii: $t = -0.01$; iii: $t = +0.01$; iv: $t = +0.1$. Dashes denote the vanishing vorticity line, and the black dot is the isolated intensity critical point. The vortices for different values of t are grayshaded differently. Figure based on Fig. 2 of Ref. 21.

This is an equation for a surface, given by height z above the critical point, on which the vortices must lie; the critical point lies on this surface, since $z = 0$ when $\boldsymbol{R}$ does.

Setting $z = 0$ in the first equation of Eqs. (8), to lowest order,

$$-2t = \boldsymbol{R} \cdot \boldsymbol{\Xi}_\perp \cdot \boldsymbol{R}, \tag{11}$$

gives the projection of the vortices in the $\boldsymbol{R}$ plane. Eq. (11) is merely the equation for an ellipse or hyperbola, depending on the sign of $\det \boldsymbol{\Xi}_\perp$: positive for ellipse (small loop, provided $t < 0$), negative for hyperbola (avoided crossing).

It is easy to find further expressions for geometric properties of these vortices, particularly with Eq. (11). For instance, with the eigenvalues of $\boldsymbol{\Xi}_\perp$,

$$\lambda_\pm \equiv \frac{1}{2}\left(\Xi_{xx} + \Xi_{yy} + \sqrt{(\Xi_{xx} - \Xi_{yy})^2 + 4\Xi_{xy}^2}\right), \tag{12}$$

the eccentricity ε of the conic section, the ($\boldsymbol{R}$-projected) area α of small loops, and the ($\boldsymbol{R}$-projected) avoidance range (closest approach) ρ of avoided crossings, are given by

$$\varepsilon = \sqrt{1 - \frac{\min(\lambda_+, \lambda_-)}{\max(\lambda_+, \lambda_-)}}, \qquad \alpha = \frac{-2t\pi}{\det \boldsymbol{\Xi}_\perp}, \qquad \rho = 2\sqrt{\frac{-2t}{\lambda_{(-\operatorname{sign} t)}}}. \tag{13}$$

The statistics of these quantities play an important role in the scalings of the previous section: the distribution of the avoidance range ρ will determine to what extent the vortex lines are self avoiding, and the distribution of α will determine the loop size distribution for small loops.

We referred above to the analogy between vanishing-vorticity lines and L line polarization singularities. Mathematically, the L line-type singularity is a defect of three-dimensional complex vector fields,[8] with rather complicated local geometry (reflected in the complexity of the formulas for avoided crossings and small loops above)[39, 48]; in three-dimensional polarization fields, the complex vector is merely the electric vector $\boldsymbol{E}$. Complex vector fields have another type of singularity, called C lines in polarization fields[39, 48]; their analogue in the gradient field of complex scalar fields was referred to as *anisotropy C lines* in Ref. 9, where their properties and

effects on vortices were described. (Anisotropy) C lines are defined as the locus where the vector $\boldsymbol{Z}$ of Eq. (4) is 'circularly polarized', that is, $\boldsymbol{Z}$ is a null vector (isotropic vector), where the complex scalar quantity

$$\varphi \equiv \boldsymbol{Z} \cdot \boldsymbol{Z} = (X^2 - Y^2) + 2\,\mathrm{i}\,\boldsymbol{X} \cdot \boldsymbol{Y} = u + \mathrm{i}\,v \tag{14}$$

is zero. The direction of the anisotropy C line, being simply a vortex, is given by $\boldsymbol{U} \times \boldsymbol{V}$, where $\boldsymbol{U} \equiv \nabla u, \boldsymbol{V} \equiv \nabla v$.

4. ANALYTIC RESULTS FOR ISOTROPIC RANDOM FIELDS

This section contains descriptions and calculations of analytic statistical densities related to the singularities discussed in the previous section: densities for vortex lines, intensity critical points (and associated small loop and avoided crossing quantities), vanishing-vorticity lines and anisotropy C lines. Rather than using the paraxial random field model,[10] where the field statistics is anisotropic (different in propagation direction and transverse plane), the calculations here use the isotropic random wave model,[11] whose statistical symmetry allow great simplifications in the calculations. Unfortunately, the most interesting of these quantities, namely those related to the topology changing events, have not been calculated at this time, due to the difficulty of the integrals.

The details of the gaussian random fields used for these calculations is standard[1, 2, 31–33] and has been often used in calculations of optical singularities in random fields[8–11, 48]; interested readers are referred to the cited literature. The model may be considered as the superposition of plane waves with uniformly random phases and directions (directions in three dimensions here), in the limit of arbitrarily many waves; the ensemble probability density function of the field and its derivatives is a multivariate gaussian, which is also the spatial probability density function since the model is ergodic. Such ensemble averages are denoted $\langle \bullet \rangle$. The distribution depends purely on the spectrum of the wavenumbers in the isotropic three-dimensional superposition, which in our simulations discussed earlier (which were only isotropically random in two dimensions) was given by a gaussian with width K_σ; for the calculations here, only moments of the spectrum will be required. The nth spectral moment will be denoted k_n; in particular, for a monochromatic superposition of waves of wavenumber k, $k_n = k^n$. As previously,[8, 33, 36] spectral moments for isotropic two-dimensional superpositions are written K_n. Relevant three-dimensional field correlations, which appear in the probability density functions, are

$$\langle \xi^2 \rangle = 1, \quad \langle \xi_i^2 \rangle = -\langle \xi \xi_{ii} \rangle = k_2/3, \quad \langle \xi_{ii}^2 \rangle = k_4/5, \quad \langle \xi_{ij}^2 \rangle = \langle \xi_{ii} \xi_{jj} \rangle = k_4/15, i \neq j. \tag{15}$$

The vortex line density in the isotropic random wave model is[11]

$$d_{\text{vortex lines}} = \langle \delta(\xi)\delta(\eta)|\boldsymbol{X} \times \boldsymbol{Y}| \rangle = k_2/3\pi. \tag{16}$$

The vortex point density in any plane is half of this line density in space,[11, 33] and so is $k_2/6\pi$, equivalent to $K_2/4\pi$, agreeing with the earlier Eq. (1).

Calculation of the density of intensity critical points is rather more difficult. The required average can be written

$$d_{\text{intensity critical points}} = \langle \delta^{*3}(\nabla|\psi|^2)|\det \partial_{ij}|\psi|^2| \rangle, \tag{17}$$

where δ^* excludes the possibility that $\psi = 0$, so only picks up the generic intensity critical points (since $\psi \neq 0$ generically when $\nabla|\psi|^2 = 0$). However, even with choices of coordinates and gauge of the previous section, this average has foiled all attempts at calculation, due to the sixth-order term in the modulus. Without this, we cannot evaluate analytically the probability density of small loops (area α) and avoided crossings (range ρ) of Eq. (13), which are, in the form of Eq. (17),

$$\begin{aligned} P_{\text{small loop}}(\alpha_0) &= \langle \delta^{*3}(\nabla|\psi|^2)|\det \partial_{ij}|\psi|^2|\,\Theta(\det \boldsymbol{\Xi}_\perp)\delta(\alpha_0 - \alpha) \rangle / d_{\text{intensity critical points}}, \\ P_{\text{avoided crossing}}(\rho_0) &= \langle \delta^{*3}(\nabla|\psi|^2)|\det \partial_{ij}|\psi|^2|\,\Theta(-\det \boldsymbol{\Xi}_\perp)\delta(\rho_0 - \rho) \rangle / d_{\text{intensity critical points}}, \end{aligned} \tag{18}$$

where α and ρ are given in Eq. (13). This difficulty in our calculations was reflected in the calculations of the density of critical points in two-dimensional speckle patterns,[49] whose final two integrals had to be found numerically.

Nevertheless, a similar calculation was made in Ref. 22, for the distribution of avoided crossing range of nodal lines in real two-dimensional monochromatic random functions, with result (scaled with $k = 1$):

$$P_{\text{2D avoided crossings}}(\rho) = \frac{6144\sqrt{3}\rho(8-\rho^2)(16-\rho^2)}{(512-64\rho^2+3\rho^4)^{5/2}}, \qquad 0 < \rho < 2\sqrt{2}. \tag{19}$$

This distribution has expectation value 1.80, vanishes when $\rho = 0$, and depends linearly on ρ for small ρ. We might expect similar behavior for the distribution of the vortex avoided crossing range of Eq. (18), justifying our observation that random vortex lines scale like random walks, rather than self-avoiding random walks. In the waves considered in Ref. 22, the nodal line loops have a minimum area of $4\pi/k^2$ (approximating to Krahn's theorem), which is different from vortex loops, which have no restriction on size;[5] care should therefore be taken in using the two-dimensional real monochromatic field results for three-dimensional complex vortices.

Although it is not possible to go further with calculations associated with small loops and avoided crossings, it is possible, without too much effort, to calculate the densities of the related vanishing vorticity lines and anisotropy C lines, using the same arguments as was used in deriving the densities of their polarization analogs.[48] These calculations are of independent interest, due to the curious numerical closeness, in the polarization case, of these densities to each other and the vortex density (16).[33, 48] The anisotropy C line density is the density of zeros of the complex scalar φ of Eq. (14), similar in form to the vortex density (16). Deferring details of the calculation to the appendix,

$$d_{\text{C, scalar}} = \langle \delta(u)\delta(v)|\boldsymbol{U}\times\boldsymbol{V}|\rangle = \frac{k_4}{k_2}\frac{\sqrt{2}}{5\pi}(\sqrt{2}+\operatorname{arcsinh}1) \approx 0.2067\frac{k_4}{k_2}. \tag{20}$$

The density of the vanishing-vorticity lines is rather more complicated, both geometrically and in its calculation (the final integral can only be done numerically), as with its polarization L line counterpart. Following Ref. 48, and the present Section 3, we choose coordinates such that $\boldsymbol{\Omega} = 0$ at the origin, with $\boldsymbol{X}||\boldsymbol{Y}||\hat{\boldsymbol{z}}$. Then, with $\boldsymbol{A} \equiv -X\nabla\eta_y + Y\nabla\xi_y$ and $\boldsymbol{B} \equiv X\nabla\eta_x - Y\nabla\xi_x$, we have

$$d_{\text{L, scalar}} = \left\langle \frac{\delta(\boldsymbol{\Omega})}{\pi|\boldsymbol{\Omega}|}|\boldsymbol{A}\times\boldsymbol{B}| \right\rangle \approx 0.219342\frac{k_4}{k_2}, \tag{21}$$

with details of the calculation in the appendix.

These two densities are rather close to each other numerically: $d_{\text{C, scalar}}/d_{\text{L, scalar}} \approx 0.942252$. Furthermore, they can be compared to the densities of the corresponding polarization singularities, namely

$$\frac{d_{\text{C,scalar}}}{d_{\text{C,polarization}}} = \frac{2\sqrt{6}(\sqrt{2}+\operatorname{arcsinh}1)}{3\sqrt{3}+2\pi}\frac{k_4}{k_2^2} \approx 0.9797\frac{k_4}{k_2^2}, \quad \frac{d_{\text{L,scalar}}}{d_{\text{L,polarization}}} \approx 1.02688\frac{k_4}{k_2^2}, \tag{22}$$

i.e. the numerical factor in each agrees to within less than 3%. This close agreement is followed by the fact that the numerical factor in the ratio of $d_{\text{C,scalar}}$ and $d_{\text{L,scalar}}$ to $d_{\text{vortex lines}}$ is close to 2 (in fact, it is 1.948 and 2.067 respectively). As mentioned in Refs. 33, 48, the origin of these numerical closenesses is obscure.

5. CONCLUDING REMARKS

We have discussed the main results so far of our simulation of three-dimensional speckle patterns, published in Ref. 4: the apparent brownian fractality of infinite optical vortex lines, and the scaling of closed vortex loop sizes. Our main results there, as already stated, were the apparent brownian fractality of the infinite periodic vortex lines, and the brownian fractality plus scale invariance of the distribution of closed loop lengths. We have also discussed the dependence of these to results on the local geometry of small vortex loops and avoided crossings, but we have been unable to estimate the distribution of these based on analytic statistics in the three-dimensional random wave model. However, we have presented new calculations of the statistical density of vanishing-vorticity lines and anisotropy C lines in the same model.

Clearly, the two numerical results above represent only the beginning of a systematic exploration of the random, large-scale configuration of optical vortices in propagating random optical fields. For instance, how

often are vortex loops threaded by other vortices, or linked, or knotted? Our preliminary investigations have found a few examples of threaded loops, but so far no links or knots. Closed loop random walks of a given knot type have the surprising property of scaling like self-avoiding walks, although the underlying process is not.[44] If we were to find statistically significant samples of knots in our superpositions, this might be a further, stronger test of brownian fractality for optical vortices, as well as being able to find other measures of computing the tangledness of the configuration, as has been useful for vortices in superfluids.[28]

The connection with the $\mathbb{Z}_3$ model is of independent interest, and we need to compare the results of our optical simulations with other results from this model (such as the scaling of loops with respect to the perimeter of their bounding cuboid[38]). Furthermore, we should test whether choosing period sizes for the supporting lattice changes any of the results – in particular, if the results are closer to those of vortices with the same shape as our (scaled) Talbot cube.

We have not discussed here the other main result of Ref. 4, namely the agreement on comparatively small sizes of the vortex structure in simulated and experimental speckle. We still do not know whether optical vortex lines in experimental patterns have the same remarkable scaling found numerically; such an experiment would have to scan extremely large volumes, without necessarily the benefit of periodicity. Of course, vortex lines only represent places of perfect destructive interference, and speckle is interspersed with regions of low intensity also (which are often experimentally difficult to distinguish from the vortices); whether these regions have characteristic fractality remains an open question.

We have been unable to calculate analytically the density of small vortex loops and avoided crossings. However, we have enough simulation data to attempt to estimate this numerically, at least insofar as to establish whether our estimate based on Eq. (19) are correct: that there is linear (or lower) behavior in ρ, so as not to give some form of repulsion between vortex lines (which would lead to self-avoiding walk scaling).

Finally, we comment that there are examples of remarkable numerical similarities in the statistical densities of nodal structures sharing some geometric similarity. Although the computed values of $d_{\mathrm{C,\ scalar}}$ and $d_{\mathrm{L,\ scalar}}$ are somewhat close, their agreement is less than the examples discussed in Ref. 33.

APPENDIX A. DETAILS OF STATISTICAL CALCULATIONS

In this section, details are outlined of the calculations of anisotropy C lines and vanishing vorticity lines, for three-dimensional isotropic gaussian random fields, resulting in the numbers given in Eqs. (20) and (21). These calculations are rather similar in form to the C line and L line density calculations for isotropic random polarization fields.[48]

A.1. Anisotropy C line density (20)

This calculation follows closely the arguments of Ref. 48 Section 5 and Appendix C. The density can be written

$$d_{\mathrm{C}} = \int \mathrm{d}^3\boldsymbol{X}\,\mathrm{d}^3\boldsymbol{Y}\,P(\boldsymbol{X},\boldsymbol{Y})\delta(X^2-Y^2)\delta(2\boldsymbol{X}\cdot\boldsymbol{Y})\int \mathrm{d}^3\boldsymbol{U}\,\mathrm{d}^3\boldsymbol{V}\,P(\boldsymbol{U},\boldsymbol{V};\boldsymbol{X},\boldsymbol{Y})|\boldsymbol{U}\times\boldsymbol{V}|, \tag{23}$$

; where $P(\boldsymbol{U},\boldsymbol{V};\boldsymbol{X},\boldsymbol{Y})$ is the probability density of vectors $\boldsymbol{U},\boldsymbol{V}$ conditional on the vectors $\boldsymbol{X},\boldsymbol{Y}$:

$$P(\boldsymbol{U},\boldsymbol{V};\boldsymbol{X},\boldsymbol{Y}) = \langle\delta(\boldsymbol{U}-\nabla u)\delta(\boldsymbol{V}-\nabla v)\rangle_{\{\boldsymbol{X},\boldsymbol{Y}\}}. \tag{24}$$

Concentrating on evaluating this latter probability density function, we have

$$\begin{aligned} P(\boldsymbol{U},\boldsymbol{V};\boldsymbol{X},\boldsymbol{Y}) &= \frac{1}{(2\pi)^6}\int \mathrm{d}^3\boldsymbol{s}\,\mathrm{d}^3\boldsymbol{t}\,\exp(-\mathrm{i}\,\boldsymbol{U}\cdot\boldsymbol{s}-\mathrm{i}\,\boldsymbol{V}\cdot\boldsymbol{t})\langle\exp(\mathrm{i}\,\boldsymbol{\nabla u}\cdot\boldsymbol{s}+\mathrm{i}\,\nabla v\cdot\boldsymbol{t})\rangle_{\{\boldsymbol{X},\boldsymbol{Y}\}} \\ &= \frac{1}{(2\pi)^6}\int \mathrm{d}^3\boldsymbol{s}\,\mathrm{d}^3\boldsymbol{t}\,\exp(-\mathrm{i}\,\boldsymbol{U}\cdot\boldsymbol{s}-\mathrm{i}\,\boldsymbol{V}\cdot\boldsymbol{t}-T/2), \end{aligned} \tag{25}$$

where

$$T \equiv \langle(\boldsymbol{\nabla u}\cdot\boldsymbol{s}+\mathrm{i}\,\nabla v\cdot\boldsymbol{t})^2\rangle_{\{\boldsymbol{X},\boldsymbol{Y}\}} = 4\,[(s_is_k+t_it_k)(X_jX_l+Y_jY_l)\langle\xi_{ij}\xi_{kl}\rangle] \tag{26}$$

(following the summation convention).

We now anticipate the δ-functions in Eq. (23). Choosing cartesian coordinates, we set $\boldsymbol{X} = \{X, 0, 0\}, \boldsymbol{Y} = \{0, X, 0\}$. Thus

$$T = \frac{8k_4}{15} X^2 (2(s_1^2 + s_2^2 + t_1^2 + t_2^2) + s_3^2 + t_3^2). \tag{27}$$

This equation is similar in form (but not in detail) to Eq. (5.7) of Ref. 48. With this choice, Eq. (25) becomes

$$\begin{aligned} P(\boldsymbol{U}, \boldsymbol{V}; \boldsymbol{X}, \boldsymbol{Y}) &= \frac{1}{(2\pi)^6} \int \mathrm{d}^3\boldsymbol{s} \, \exp\left(-\mathrm{i}\, \boldsymbol{U} \cdot \boldsymbol{s} - \frac{1}{2} \frac{8k_4 X^2}{15} (2(s_1^2 + s_2^2) + s_3^2) \right) \\ &\qquad \times \text{same with } \{\boldsymbol{V}, \boldsymbol{t}\} \text{ for } \{\boldsymbol{U}, \boldsymbol{s}\} \\ &= \frac{1}{4(2\pi)^3} \left(\frac{15}{8k_4 X^2} \right) \exp\left(-\frac{1}{2} \frac{15}{16k_4 X^2} (s_1^2 + s_2^2 + 2s_3^2 + t_1^2 + t_2^2 + 2t_3^2) \right) \end{aligned} \tag{28}$$

This is then substituted into the overall density formula (23). With $\boldsymbol{X}, \boldsymbol{Y}$ written in polar coordinates, and trivial quantities integrated,

$$\begin{aligned} d_{\mathrm{C}} &= \frac{16\pi^2}{(2\pi)^6} \left(\frac{3}{k_2} \right)^3 \left(\frac{15}{16k_4} \right)^3 \int_0^\infty \mathrm{d}X \int_0^\infty \mathrm{d}Y \int_0^\pi \mathrm{d}\theta \, \frac{X^2 Y^2 \sin\theta}{X^6} \frac{\delta(X - Y)}{X + Y} \frac{\cos\theta}{2XY} \exp\left(-\frac{1}{2} \frac{3}{k_2} (X^2 + Y^2) \right) \\ &\qquad \times \int \mathrm{d}^3\boldsymbol{U} \, \mathrm{d}^3\boldsymbol{V} |\boldsymbol{U} \times \boldsymbol{V}| \exp\left(-\frac{1}{2} \frac{15}{16k_4 X^2} (U^2 + V^2 + U_3^2 + V_3^2) \right). \end{aligned} \tag{29}$$

$\boldsymbol{U}$ is rescaled to $\boldsymbol{U}\sqrt{15/16k_4X^2}$, and similarly for $\boldsymbol{V}$, and X, Y, θ are integrated. d_{C} can therefore be expressed in terms only of the $\boldsymbol{U}, \boldsymbol{V}$ integrals,

$$d_{\mathrm{C}} = \frac{1}{10\pi^4} \frac{k_4}{k_2} \int \mathrm{d}^3\boldsymbol{U} \, \mathrm{d}^3\boldsymbol{V} |\boldsymbol{U} \times \boldsymbol{V}| \exp\left(-\frac{U^2 + V^2 + U_3^2 + V_3^2}{2} \right). \tag{30}$$

This is integrated can be done by expressing the modulus as a Fourier integral, leading to quadratic imaginary terms in $\boldsymbol{U}, \boldsymbol{V}$. These can be integrated as a regular gaussian, resulting in an integral over Fourier variables r, t :

$$d_{\mathrm{C}} = \frac{128\pi^2}{10\pi^4} \frac{k_4}{k_2} \int_0^\infty \mathrm{d}r \int \mathrm{d}t \, \frac{r(1 - t^2)}{(t^2 + r^2)(2 + r^2 + 2t^2)^3} = \frac{2}{25\pi^2} \frac{k_4}{k_2} \int \mathrm{d}t \, [g(t) + h(t)] \tag{31}$$

where

$$g(t) = \frac{(t^2 - 1)(6 + 5t^2)}{(1 + t^2)^2 (2 + t^2)^2}, \qquad h(t) = \frac{8(1 - t^2) \log(2(1 + t^2)/t^2)}{(2 + t^2)^3} \tag{32}$$

These are integrated using complex plane methods, in a similar way to the related integrals in Ref. 48, resulting in the solution Eq. (20).

A.2. Vanishing vorticity line density ($\boldsymbol{\Omega = 0}$ line density) (21)

This calculation follows closely the arguments of Ref. 48 Section 6 and Appendix D. We define

$$\boldsymbol{W} \equiv \{X\eta_{xx} - Y\xi_{xx}, X\eta_{yy} - Y\xi_{yy}, X\eta_{xy} - Y\xi_{xy}, X\eta_{xz} - Y\xi_{xz}, X\eta_{yz} - Y\xi_{yz}\}, \tag{33}$$

where $\boldsymbol{A} = \{-V_3, -V_2, -V_5\}$ and $\boldsymbol{B} = \{V_1, V_3, V_4\}$. Also, we introduce a 5×5 matrix $\boldsymbol{\Lambda}$ such that $\boldsymbol{A} \times \boldsymbol{B} = \boldsymbol{W} \cdot \boldsymbol{\Lambda} \cdot \boldsymbol{W}$. The distribution of $\boldsymbol{W}$ conditional on $\boldsymbol{X}$ and $\boldsymbol{Y}$ is

$$P(\boldsymbol{W}; \boldsymbol{X}, \boldsymbol{Y}) = \langle \delta(\boldsymbol{W} - (X\eta_{\bullet\bullet} - Y\xi_{\bullet\bullet})) \rangle_{\{\boldsymbol{X}, \boldsymbol{Y}\}} = \frac{1}{(2\pi)^5} \int \mathrm{d}^5\boldsymbol{t} \, \exp(-\mathrm{i}\, \boldsymbol{t} \cdot \boldsymbol{W} - F/2), \tag{34}$$

with

$$F = \langle [\boldsymbol{t} \cdot (X\eta_{\bullet\bullet} - Y\xi_{\bullet\bullet})]^2 \rangle = \frac{k_4(X^2 + Y^2)}{15} (3(t_1^2 + t_2^2) + 2t_1 t_2 + t_3^2 + t_4^2 + t_5^2) = k_4(X^2 + Y^2) \boldsymbol{t} \cdot \boldsymbol{\Xi} \cdot \boldsymbol{t}, \tag{35}$$

which defines the symmetric matrix $\boldsymbol{\Xi}$ from the quadratic form. Thus

$$P(\boldsymbol{W};\boldsymbol{X},\boldsymbol{Y}) = \frac{1}{(2\pi)^{5/2}} \frac{1}{k_4^{5/2}(X^2+Y^2)^{5/2}} \frac{225\sqrt{15}}{2\sqrt{2}} \exp\left(-\frac{\boldsymbol{W}\boldsymbol{\Xi}^{-1}\cdot\boldsymbol{W}}{2k_4(X^2+Y^2)}\right). \tag{36}$$

The vanishing-vorticity line density can therefore be written

$$\begin{aligned} d_{\mathrm{L}} &= \frac{1}{(2\pi)^3}\left(\frac{3}{k_2}\right)^3 \int \mathrm{d}^3\boldsymbol{X}\,\mathrm{d}^3\boldsymbol{Y}\, \frac{\delta(|\boldsymbol{X}\times\boldsymbol{Y}|)}{\pi|\boldsymbol{X}\times\boldsymbol{Y}|} \exp\left(-\frac{X^2+Y^2}{2k_2/3}\right) \\ &\quad \times \frac{225\sqrt{15}}{(2\pi)^{5/2}2\sqrt{2}k_4^{5/2}} \int \mathrm{d}^5\boldsymbol{W}\, \frac{|\boldsymbol{W}\cdot\boldsymbol{\Lambda}\cdot\boldsymbol{W}|}{(X^2+Y^2)^{5/2}} \exp\left(-\frac{\boldsymbol{W}\cdot\boldsymbol{\Xi}^{-1}\cdot\boldsymbol{W}}{2k_4(X^2+Y^2)}\right). \end{aligned} \tag{37}$$

As in the calculation of anisotropy C line density, $\boldsymbol{W}$ is rescaled to $\boldsymbol{W}/\sqrt{K_4(X^2+Y^2)}$. This allows integration of $\boldsymbol{X}$ and $\boldsymbol{Y}$, yielding

$$d_{\mathrm{L}} = \frac{675\sqrt{15}}{16\pi^{7/2}} \frac{k_4}{k_2} \int \mathrm{d}^5\boldsymbol{W}\, |\boldsymbol{W}\cdot\boldsymbol{\Lambda}\cdot\boldsymbol{W}| \exp\left(-\frac{\boldsymbol{W}\cdot\boldsymbol{\Xi}^{-1}\cdot\boldsymbol{W}}{2}\right). \tag{38}$$

This integral is tackled using the same strategy as before, although the resulting quadratic form from $\boldsymbol{\Lambda}$ is more complicated here. After the gaussian integral, the expression is

$$\begin{aligned} d_{\mathrm{L}} &= \frac{2700}{\pi^2}\frac{k_4}{k_2} \int_0^\infty \mathrm{d}r \int \mathrm{d}t\, \frac{r}{(t^2+r^2)\left((225+r^2+30\,\mathrm{i}\,t)(225+3r^2+8t^2-30\,\mathrm{i}\,t)\right)^{5/2}} \\ &\quad \times \left(\begin{array}{l} 56953125+810000r^2+3150r^4-3r^6-2227500t^2-2700r^2t^2-44r^4t^2+57600t^4-16r^2t^4 \\ +10631250\,\mathrm{i}\,t+54000\,\mathrm{i}\,r^2t+210\,\mathrm{i}\,r^4t-621000\,\mathrm{i}\,t^3-1200\,\mathrm{i}\,r^2t^3+960\,\mathrm{i}\,t^5 \end{array} \right) \end{aligned} \tag{39}$$

This integral can be integrated numerically, giving 0.00080178.

ACKNOWLEDGMENTS

MRD thanks Profs. Michael Berry, John Hannay, and Uzy Smilansky for useful discussions, and we thank Florian Flossmann for additional support. This work was supported by the Leverhulme Trust and the Royal Society of London.

REFERENCES

1. J. W. Goodman, in *Laser speckle and related phenomena*, J. C. Dainty, ed., pp. 9–75, Springer-Verlag, 1975.
2. J. C. Dainty, *Prog. Opt.* **14**, pp. 1–46, 1976.
3. J. W. Goodman, *Speckle Phenomena in Optics*, Ben Roberts & Co, 2006.
4. K. O'Holleran, M. R. Dennis, F. Flossmann and M. J. Padgett, *Phys. Rev. Lett.* in press, 2008.
5. J. F. Nye and M. V. Berry, *Proc. R. Soc. Lond. A* **336**, pp. 165–190, 1974.
6. M. V. Berry, in *Les Houches Session XXV - Physics of Defects*, K. R. Balian and J.-P. Poirier, eds., pp. 453–543, North-Holland, Amsterdam, 1981.
7. J. F. Nye, *Natural focusing and fine structure of light*, Institute of Physics Publishing, Bristol, 1999.
8. M. R. Dennis, *Topological singularities in wave fields*. Ph. D. thesis, Bristol University, 2001.
9. M. R. Dennis, *J. Opt. A:Pure App. Opt.* **6**, pp. S202–S208, 2004.
10. M. V. Berry, *J. Phys. A:Math. Gen.* **11**, pp. 27–37, 1978.
11. M. V. Berry and M. R. Dennis, *Proc. R. Soc. Lond. A* **456**, pp. 2059–2079, 2000. (errata **456** 3059).
12. M. V. Berry, *SPIE Proc.* **3487**, pp. 1–15, 1998.
13. M. V. Berry and M. R. Dennis, *Proc. R. Soc. Lond. A* **457**, pp. 2251–2263, 2001.
14. M. V. Berry and M. R. Dennis, *J. Phys. A:Math. Gen.* **34**, pp. 8877–8888, 2001.
15. J. Leach, M. R. Dennis, J. Courtial and M. J. Padgett, *Nature* **432**, p. 165, 2004.

16. J. Leach, M. R. Dennis, J. Courtial and M. J. Padgett, *New J. Phys.* **7**, 55, 2005.
17. M. R. Dennis, *New J. Phys.* **5**, 134, 2003.
18. G. Molina-Terriza, J. Recolons, J. P. Torres, L. Torner and E. M. Wright, *Phys. Rev. Lett.* **87**, 023902, 2001.
19. J. F. Nye, *J. Opt. A:Pure App. Opt.* **6**, pp. S251–S254, 2004.
20. K. O'Holleran, M. J. Padgett and M. R. Dennis, *Opt. Exp.* **14** pp. 3039–3044, 2006.
21. M. V. Berry and M. R. Dennis, *J. Phys. A:Math. Theor.* **40**, pp. 65–74, 2007.
22. A. G. Monastra, U. Smilansky and S. Gnutzmann, *J. Phys. A:Math. Gen.* **36**, pp. 1845–1853, 2003.
23. K. O'Holleran, M. R. Dennis and M. J. Padgett, *JEOS-RP* **1**, 06008, 2006.
24. K. W. Schwarz, *Phys. Rev. B* **38**, pp. 2398–2417, 1988.
25. W. F. Vinen and J. J. Niemela, *J. Low Temp. Phys.* **128**, pp. 167–231, 2002.
26. D. Kivotides, C. F. Barenghi and D. C. Samuels, *Phys. Rev. Lett.* **87**, 155301, 2001.
27. T. Araki, M. Tsubota and S. K. Nemirovskii, *Phys. Rev. Lett.* **89**, 145301, 2002.
28. D. R. Poole, H. Scoffield, C. F. Barenghi and D. C. Samuels, *J. Low Temp. Phys.* **132**, pp. 97-117, 2003.
29. A. Mitani and M. Tsubota, *Phys. Rev. B* **74**, 024526, 2006.
30. M. B. Hindmarsh and T. W. B. Kibble, *Rep. Prog. Phys.* **58**, pp. 477–562, 1995.
31. B. I. Halperin, in *Les Houches Session XXV - Physics of Defects*, K. R. Balian and J.-P. Poirier, eds., pp. 813–857, North-Holland, Amsterdam, 1981.
32. M. V. Berry, *J. Phys. A:Math. Gen.* **10**, pp. 2083–2091, 1977.
33. M. R. Dennis, *Eur. Phys. J. Special Topics* **145**, pp. 191–210, 2007.
34. H. F. Talbot, *Phil. Mag.* **9**, pp. 401–407, 1836.
35. K. Patorski, *Prog. Opt.* **27**, pp. 1–108, 1989.
36. M. R. Dennis, *SPIE Proc.* **4403**, pp. 13–23, 2001.
37. R. C. Bourret, *Nuov. Cim* **18**, pp. 347–356, 1960.
38. T. Vachaspati and A. Vilenkin, *Phys. Rev. D* **30**, pp. 2036–2045, 1984.
39. J. F. Nye and J. V. Hajnal, *Proc. R. Soc. Lond. A* **409**, pp. 21–36, 1987.
40. K. Falconer, *Fractal Geometry: Mathematical Foundations and Applications*, John Wiley & Sons, 1990.
41. e.g. E.W. Weisstein, "Pólya's Random Walk Constants." From *MathWorld–A Wolfram Web Resource.* `http://mathworld.wolfram.com/PolyasRandomWalkConstants.html`.
42. B. Nienhuis, *J. Stat. Phys.* **34**, pp. 731–761, 1984.
43. J. C. Le Guillou and J. Zinn-Justin, *Phys. Rev. Lett.* **39**, pp. 95–98, 1977.
44. A. Dobay, J. Dubochet, K. Millett, P.-E. Sottas and A. Stasiak, *Proc. Nat. Acad. Sci. U. S. A.* **100**, pp. 5611–5615, 2003.
45. E. Bogomolny and C. Schmit, *Phys. Rev. Lett.* **88**, 114102, 2002.
46. G. Foltin, *arXiv* nlin.CD/0302049, 2003.
47. E. Bogomolny and C. Schmit, *J. Phys. A: Math. Theor.* **40**, pp. 14033–14043, 2007.
48. M. V. Berry and M. R. Dennis, *Proc. R. Soc. Lond. A* **457**, pp. 141–155, 2001.
49. A. Weinrib and B. I. Halperin, *Phys. Rev. B* **26**, pp. 1362–1368, 1982.